Available online at www.sciencedirect.com
ScienceDirect
Wear 262 (2007) 1490–1495
WEAR
www.elsevier.com/locate/wear

Cumulative damage modeling of solid lubricant coatings that experience wear and interfacial fatigue

N.L. McCook, D.L. Burris, N.H. Kim, W.G. Sawyer *

Department of Mechanical and Aerospace Engineering, University of Florida, Gainesville, FL 32611, United States

Received 31 May 2006; received in revised form 12 January 2007; accepted 17 January 2007
Available online 23 March 2007

Abstract

Solid lubricating coatings comprise a large segment of tribological materials and under a spherical contact the coating/substrate interface experiences cyclic shear stress that leads to delamination of the coatings from the substrate and premature failure. The polymeric solid lubricating coating used in this study is an expanded PTFE/epoxy composite. The coatings experience cumulative damage caused by interfacial fatigue and wear ultimately leading to failure. Using a finite element simulation of the contact conditions and experimental data, a numerical analysis of the coupled failure modes was completed. The results of the modeling offer insight to designers on considerations in extending the lives of coatings subject to cyclic stresses. The experimental data for cycles to failure versus coating thickness fall closely to the fit for the cumulative damage model. This result also shows that these coatings experience failure primarily from interfacial fatigue under these pin-on-disk experimental conditions.

Keywords: Solid lubricants; Coatings; Life prediction; Wear; Delamination; PTFE; Epoxy

1. Introduction

Friction coefficients and wear rates are often characterized using specially constructed apparatuses for component level testing; the geometries, kinematics and loads are nominally equivalent to those seen in a target application. However, rather standardized tribometers such as pin-on-disk tribometers are frequently used during materials development activities. Typically, the conditions at the tribological interface are selected to closely approximate the conditions found in an application area. This would involve attempts to match contact pressure, sliding speed, ambient temperature, environment, and many more variables that are determined to be important to the material system. The subsurface stress state is rarely matched to the target application in pin-on-disk testing and these stresses and fatigue can be the dominant failure mode of tribological coatings tested on such apparatuses.

Coatings comprise a large segment of tribological materials. Often, engineers are concerned with the life and/or abrasive wear resistance of a coating. Pin-on-disk machines using high speed and precision spindles have the ability to accumulate large numbers of sliding cycles quickly under high circular contact stresses. An efficient experimental protocol is to run the sample until the coating fails or all of the material is removed from the wear track. A spike in the friction coefficient is often used to determine when this event occurred. At the completion of the experiment the wear volume is calculated using coating thickness and pin geometry (such a technique is reasonable if the coating simply wore through to the substrate material). Under a sliding circular contact with a very wear resistant material fatigue of a coating/substrate interface can lead to a delamination event where the coating is rapidly removed after a long initiation and crack propagation process.

This coupling of wear and delamination is an interesting problem [1–3]. When modeling the disk surface of a circular contact both the wear and fatigue damage accumulate each cycle. This presents an interesting coupled problem [4–6] because the gradual removal of material from the coating surfaces due to wear changes the subsurface stress distribution, which drives the fatigue and delamination process. This paper presents a numerical technique for this coupled problem and compares the model to data collected on a unique and very wear resistant solid lubricating polymeric coating. The equations used here are empirical, based on the specific material properties, bonding technique and

* Corresponding author. Tel.: +1 352 392 8488; fax: +1 352 392 1071.
E-mail address: wgsawyer@ufl.edu (W.G. Sawyer).

0043-1648/$ – see front matter © 2007 Elsevier B.V. All rights reserved.
doi:10.1016/j.wear.2007.01.042

contact geometry used in this study and therefore only apply to this study. However, the experimental methods by which these equations were obtained and the subsequent numerical procedure are completely general and may be used to predict life in a variety of other systems.

2. Materials

Composite films used in this study are comprised of approximately 30–50 weight percent epoxy in expanded PTFE [7]. The epoxy filler strengthens the composite and provides a direct bond to the substrate; the PTFE provides material for transfer films and a low shear film at the tribological interface. Nanoindentation is used to calculate an average coating modulus of $E = 3$ GPa, with the steel having a modulus of $E = 200$ GPa. Poisson's ratios of 0.4 and 0.3 are used for the coating and steel, respectively. An experimental matrix varying the thickness of the coating from 30 to 360 μm is used to determine the sensitivity of the film failure on coating thickness, as well as a method for estimating a shear stress versus number of cycles curve for a fatigue process occurring at the coating/steel interface. The pins are made of polished 304 SS spheres with a radius of 3.2 mm. Each sample is tested until failure at which time scanning white light interferometry is used to measure the thickness of the coating. Following the method previously described a single point wear rate is then calculated.

3. Apparatus and experimental procedure

A rotating pin-on-disk tribometer [7] was used for this study. The sliding speed was $v = 1$ m/s and a dead-weight normal load of $F = 5$ N was applied. As previously mentioned, the pin was 304 SS with a radius of 3.2 mm. The friction coefficient was continuously recorded using a computer data acquisition system. The tribometer spindle is equipped with an encoder and the data acquisition system maintains a running count of the number of revolutions. At coating failure, spikes begin to occur in the friction coefficient data and exposed steel within the wear scar can be seen visually; the number of cycles to coating failure is determined from these events. The tribometer is also equipped with a displacement transducer located directly over the pin surface, which allows continuous monitoring of the gradual removal of material from the sample.

4. Finite element analysis

Axisymmetric finite element analysis was used to obtain the stress state at the interface. The coating was discretized by 50×10 mesh, while the substrate was a 50×20 mesh. In order to improve the solution accuracy, smaller element size was used near the contact region. A surface-to-surface contact modeling technique that prevents contact elements and target elements from penetrating each other was used. In this contact–target strategy, the contact pressure was only calculated for nodes on the contact elements. Thus, contact elements were generated on the coating surface, while target elements were generated on the ball [8,9].

To find the contact point locations and pressure, an augmented Lagrangian formulation was used. In this technique, the impenetrability constraint is imposed at all possible contact nodes using the Lagrange multiplier method in optimization theory. This technique possesses the stability of the penalty method but imposes the impenetrability of the Lagrange multiplier method. The contact problem becomes nonlinear even if the structure experiences a small deformation; thus, the structural equilibrium configuration is found by incrementally changing the applied load. In general, six or seven Newton–Raphson iterations are required to find the converged configuration for each load step.

In finite element analysis, the traction stresses and worn shape are neglected; i.e., a ball is assumed to contact with a flat surface, thus overestimating the stresses after large wear losses. A matrix varying the normal load from 1 to 7 N, elastic modulus of the coating from 1 to 7 GPa, and the thickness of the coating from 30 to 500 μm is completed to provide more insight on the roles of each. The shear stresses at the interfaces are determined for coatings within the tribological experimental matrix, with an elastic modulus of $E = 3$ GPa, a normal load of $F_n = 5$ N, and varying in thickness from 30 to 360 μm.

5. Results and discussion

A log–log plot of single point wear rate calculations versus coating thickness (Fig. 1) shows values varying from 10^{-3} to 10^{-8} mm^3/(N m) monotonically decreasing with increasing thickness. One might be inclined to suspect that the thicker coatings are thus more wear resistant—it should be noted that the thickest four samples did not wear through to the substrate even after tens of millions of cycles.

For the coatings used in this study, cracks initiated at the bonded interface [10] and when these cracks coalesced into large enough regions the coatings failed by debonding across

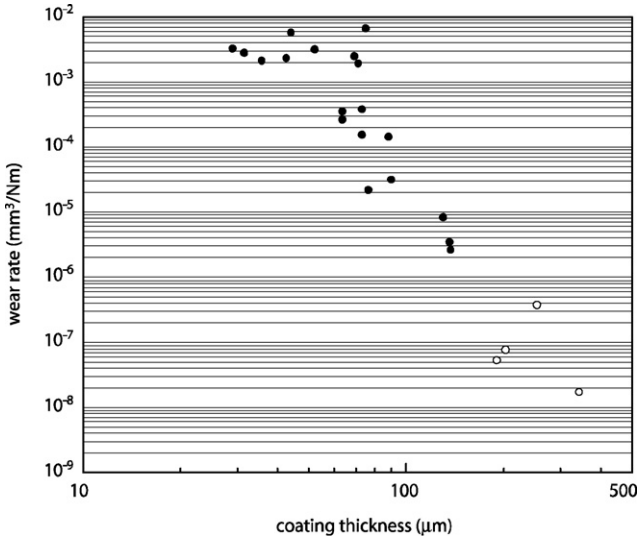

Fig. 1. Coating thickness (μm) vs. wear rate (mm^3/N m). The open circles indicate coatings that did not fail under cyclic loading and the closed circles indicate samples that were run to failure. Such coatings were run in excess on 20 million cycles.

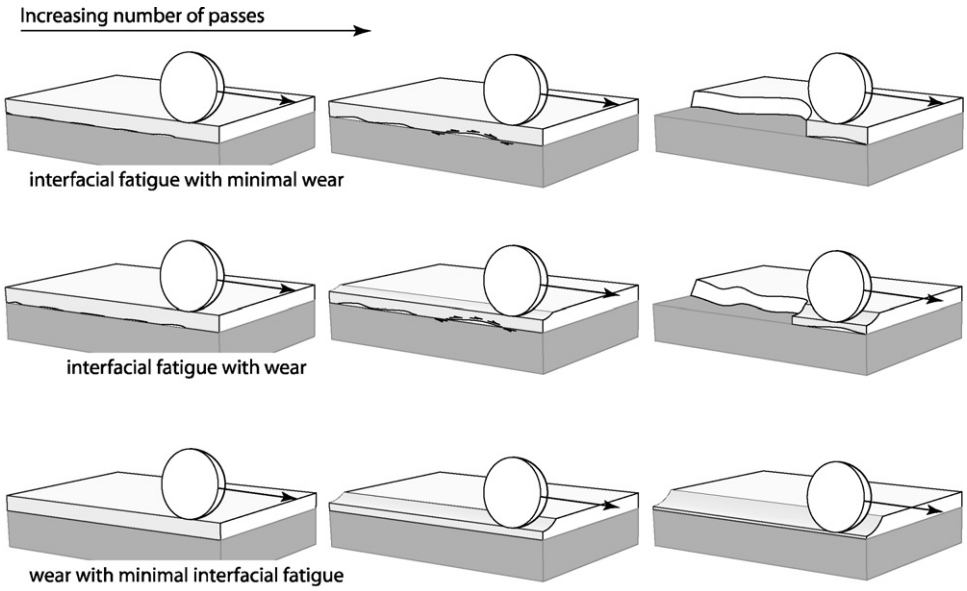

Fig. 2. Three different scenarios for the complete removal of the solid lubricant coatings. The top figure shows a process where interfacial fatigue cause film removal in the absence of wear, the middle figure shows both wear and interfacial fatigue acting together, and the final figure shows a scenario where the pin wears through the coating in the absence of interfacial fatigue.

this interface and ejected large pieces of the coating. This cyclic fatigue failure is hypothesized to result from cyclic shear stress at the bond interface. For the thin coatings delamination occurred so quickly that no measurable amounts of wear were detected. For the thicker coatings, gradual removal of coating material led to a monotonic thinning of the coating but did not initiate delamination. For all other films there is a continuous thinning of the film followed by delamination; a combination of wear and fatigue-induced failure. Fig. 2 shows a pictorial illustrating the three failure modes of the coatings under sliding: fatigue in the absence of wear, wear and fatigue, and wear in the absence of fatigue.

Finite element analyses were performed to obtain stresses at the coating/substrate interface. Fig. 4a shows contour plots of the subsurface shear stresses for the experimental conditions ($F_n = 5$ N and $E_{coating} = 3$ GPa), and as expected the maximum shear stress at the interface increases with decreasing thickness from 5 to 42 MPa for the 360 and 30 μm coatings, respectively. The contours are regions of constant shear stress with increasing stress as the color spectrum goes from dark blue to red.

The cyclic shear stress, τ, at the interface was plotted in Fig. 4b versus the coating thickness. A curve fit to this data gives a continuous function for interfacial stress as a function of the distance between the interface and the point of contact, h,

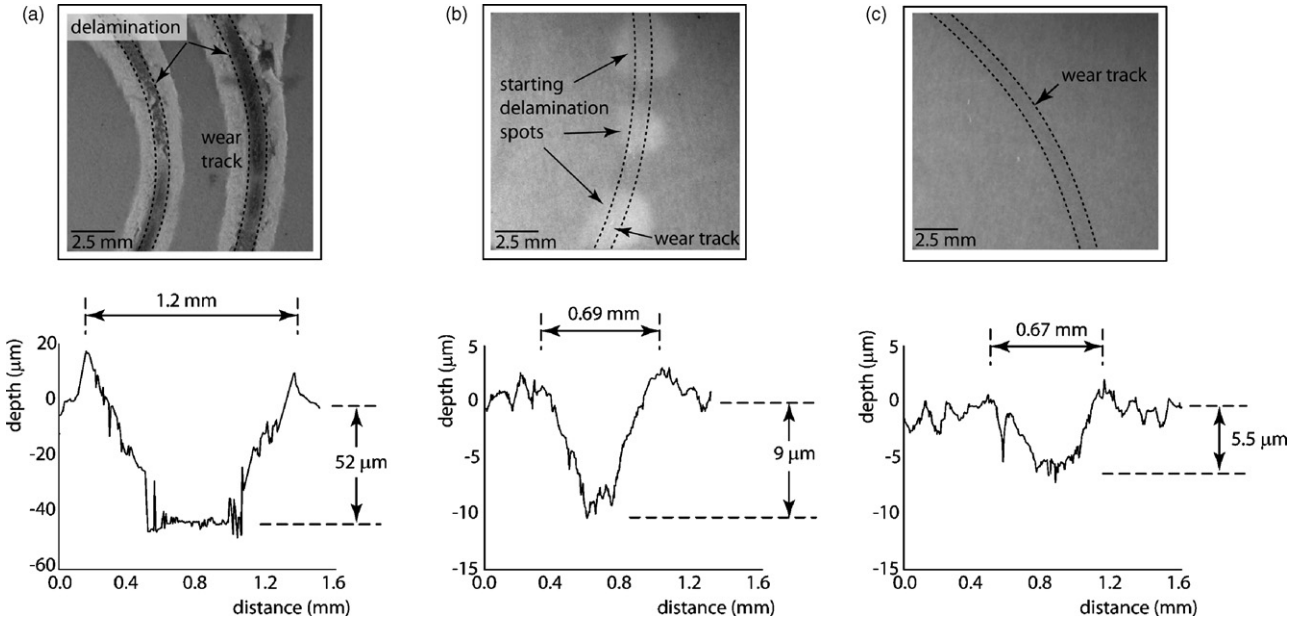

Fig. 3. Optical microscopy of a wear tracks (above) and profilometry scans across the wear tracks (below). A wear track that (a) has completely delaminated, (b) shows both wear and visible subsurface delamination, and (c) is wearing but does not show visible subsurface delamination.

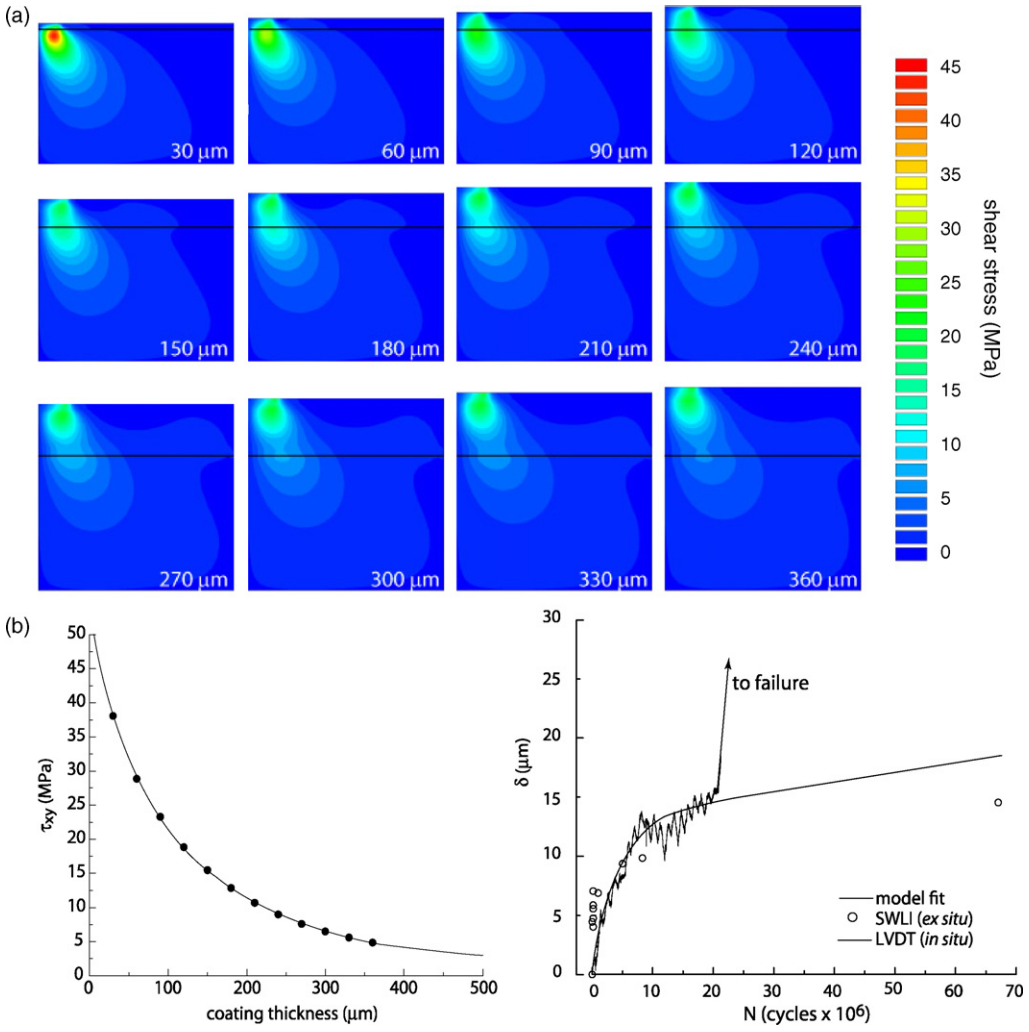

Fig. 4. Contour plots of the subsurface shear stress based on finite element analysis. The black line indicates the interface between substrate and coating. The coatings varied in thickness from 30 to 360 mm, and a 5 N load and 3 GPa elastic modulus were used in the analysis. (a) Finite element results for the maximum shear stress at the interface vs. the coating thickness. (b) The wear depth vs. number of cycles for and in situ (LVDT) and ex situ (SWLI) measurements, along with the model fit to this data. The open points are samples that wear not run to failure.

and is given in Eq (1).

$$\tau(h) = 56.9\mathrm{e}^{(-5.197(h/0.001)^{0.729})} \quad (1)$$

An in situ displacement measurement and interrupted scanning white light interferometric measurement of wear track depth, δ, for several samples are plotted as a function of cycles in Fig. 4b. Initially, the penetration rate is very high, likely a result of both the high wear rate transient period as well as a concentrated contact area. The penetration rate becomes stable around 10 million cycles. In situ displacement measurements were insensitive to coating thickness and data from a 200 μm thick coating that failed around 20 million cycles was used to fit a function for material recession as a function of number of cycles, N.

$$\delta(N) = (8 \times 10^{-8} \times N + 13)(1 - \mathrm{e}^{-(N/4\times10^6)}) \quad (2)$$

As wear occurs, δ increases and the film thickness decreases, which increase the interfacial shear stress exponentially.

Inserting the initial coating thickness into Eq. (1) gives initial interfacial shear stress, which is plotted versus cycles at failure in Fig. 5. A confounded but conservative estimate of the stress-life fatigue diagram can be obtained by assuming the samples that experienced low cycles to failure did not incur wear (200,000 cycles was the cutoff for neglecting wear). An endurance limit of 13 MPa chosen based on the regression analysis for the samples that ran-out the experiments. The corresponding expression for the fatigue-life diagram is given by Eq. (3).

$$\tau(N) = (-1.98\ \ln(N) + 47)(\mathrm{e}^{-(2.5\times10^{-8}\times N)}) + 13(1 - \mathrm{e}^{-(2.5\times10^{-8}\times N)}) \quad (3)$$

Because the shear stress at the bonded interface is an exponential function of the worn depth, and because fatigue occurs in the presence of wear, a cumulative damage model is needed to account for the continuously varying fatigue stress at the bonded interface. The Palmgren–Minor linear damage model is the simplest and most frequently used according to Collins [11]. Although this is not generally the most accurate model, a more intimate understanding of the behavior of this particular

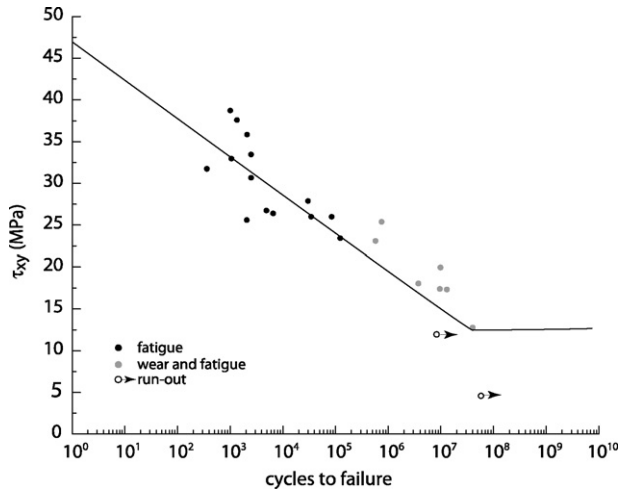

Fig. 5. Initial interfacial shear stress plotted vs. the experimental cycles at failure. A curve is fit to the samples failing less than 200,000 cycles and an endurance limit is set at 13 MPa. The samples accumulating less than 200,000 cycles were assumed to experience only fatigue, the second group experiences fatigue and wear and the run-out samples only experienced wear and did not fail.

interface would be needed to assign a more specific model. In this study, a numerical scheme using the linear damage model was implemented to incrementally calculate the wear depth and then the accumulated damage over a given cyclic interval. The accumulated damage at any cycle is thus given by Eq. (4).

$$\text{Damage} = \sum \frac{\Delta N}{N_f(\tau)} \tag{4}$$

When the accumulated damage is equal to unity, the coating is determined to have failed. Eq. (4) is solved numerically to obtain the number of cycles to failure for a coating of any thickness. This solution process is easily visualized in the form of a flow chart; this flow chart is shown in Fig. 6. The input to the model are the initial coating thickness, t_0, and the cyclic interval.

The wear depth, δ, is first calculated at the initial cycle number and then the change in thickness, h, can be calculated. Once the new thickness, h, is determined, the shear stress, τ, can be determined for that thickness. That shear stress, τ, is then checked to determine if it is above the endurance limit (in this case $\tau = 13$ MPa). If the shear stress is less than the endurance limit, the number of cycles is incremented by the cycle interval, ΔN. The values for δ, N, h, and τ are updated until the shear stress is above the endurance limit (no fatigue damage has occurred until this limit is exceeded). The number of cycles to failure, N_f, is determined for the calculated shear stress and the amount of damage at that cycle number is then calculated. The number of cycles is incremented and the process is repeated until the damage accumulates to unity.

Fig. 7a shows a plot of the number of cycles to failure versus coating thickness for the model fit using the cumulative damage model and the experimental data. Curves for the expected life of coatings with wear in the absence of fatigue and for fatigue in the absence of wear are also given. The lives of the coatings all fall closely to the predicted life, essentially because the very low wear rate of the material ($\sim$1–10 $\times$ 10^{-8} mm^3/N m) allows substantial cycles to accumulate and fatigue the interface. A more typical wear resistant material with a wear rate of 1×10^{-5} mm^3/N m (epoxy) would have equal contributions from wear and fatigue, while a less wear resistant material such as PTFE (1×10^{-3} mm^3/N m) would wear through before accumulating any fatigue damage. Fig. 7b shows this comparison of wear rates of PTFE, epoxy, and the composite coating. Having both a wear-rate and interfacial fatigue-life curves, predictions for other contact geometries and applications can be made.

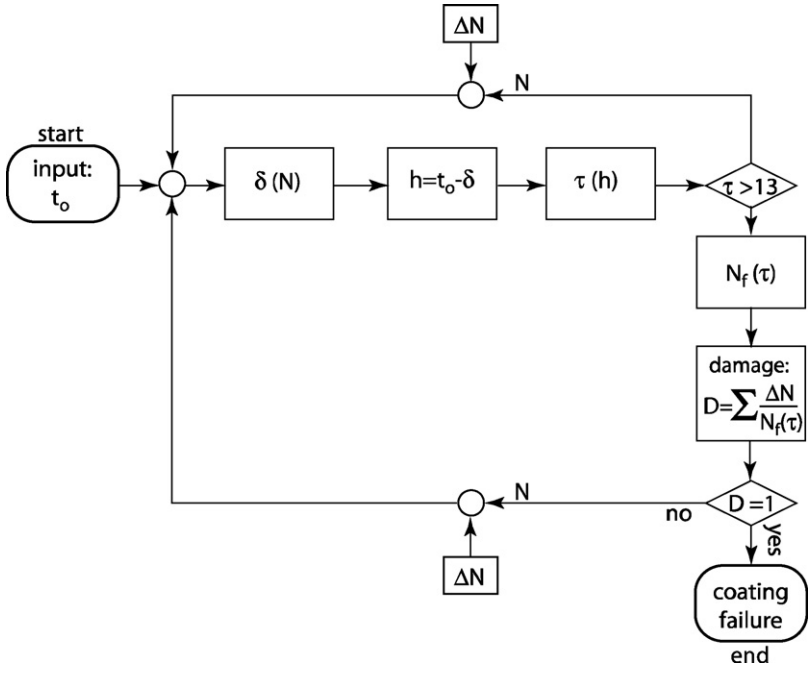

Fig. 6. Flow chart for numerical solution for life prediction based on coating thickness.

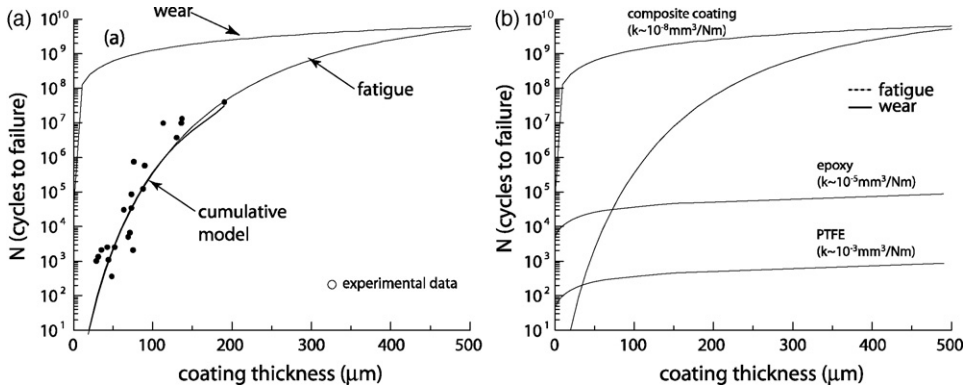

Fig. 7. (a) Plot of the number of cycles to failure vs. coating thickness for the model fit using the cumulative damage model and the experimental data. Curves for the expected life of coatings with wear in the absence of fatigue and for fatigue in the absence of wear are also given. (b) Comparison of wear rates of PTFE, epoxy, and the composite coating along with the fatigue curve.

6. Conclusions

A coupled numerical model that increments wear depth and interfacial shear stress to increment fatigue damage gives reasonable predictions for the failures of a wear resistant solid lubricating coating that was dominated by fatigue. The methodology is generic and easily applied to pin-on-disk testing data sets.

Acknowledgements

This material is based upon an AFOSR-MURI grant FA9550-04-1-0367. Any opinions, findings, and conclusions or recommendations expressed in this material are those of the authors and do not necessarily reflect the views of the Air Force Office of Scientific Research. The authors acknowledge the support from W.L. Gore for a portion of the funding for this research, and providing the ePTFE and epoxy coatings.

References

[1] N. Suh, Overview of delamination theory of wear, Wear 44 (1977) 1–16.
[2] N. Suh, Delamination theory of wear, Wear 25 (1973) 111–124.
[3] F. Kennedy, J. Currier, S. Plumet, J. Duda, D. Gestwick, J. Collier, B. Currier, M. Dubourg, Contact fatigue failure of ultra-high molecular weight polyethylene bearing components of knee prostheses, J. Tribol. T ASME 122 (2000) 332–339.
[4] W. Sawyer, Surface shape and contact pressure evolution in two component surfaces: Application to copper chemical mechanical polishing, Tribol. Lett. 17 (2004) 139–145.
[5] D. Dickrell, D. Dooner, W. Sawyer, The evolution of geometry for a wearing circular cam: analytical and computer simulation with comparison to experiment, J. Tribol. T ASME 125 (2003) 187–192.
[6] D. Dickrell, W. Sawyer, Evolution of wear in a two-dimensional bushing, Tribol. T 47 (2004) 257–262.
[7] N. Mccook, D. Burris, G. Bourne, J. Steffens, J. Hanrahan, W. Sawyer, Wear resistant solid lubricant coating made from ptfe and epoxy, Tribol. Lett. 18 (2005) 119–124.
[8] N. Kim, D. Won, D. Burris, B. Holtkamp, G. Gessel, P. Swanson, W. Sawyer, Finite element analysis and experiments of metal/metal wear in oscillatory contacts, Wear 258 (2005) 1787–1793.
[9] N. Kim, K. Choi, J. Chen, Y. Park, Meshless shape design sensitivity analysis and optimization for contact problem with friction, Comput. Mech. 25 (2000) 157–168.
[10] M. Quaresimin, M. Ricotta, Fatigue behaviour and damage evolution of single lap bonded joints in composite material, Compos. Sci. Technol. 66 (2006) 176–187.
[11] J.A. Collins, Failure of Materials in Mechanical Design, Analysis, Prediction, Prevention, second ed., John Wiley and Sons, Inc., Hoboken, NJ, 1993.